Residual Monte Carlo Transport in Time with Consistent Low-Order Acceleration for 1D Thermal Radiative Transfer

Simon R. Bolding and Jim E. Morel

Texas A&M University Nuclear Engineering Department,
sbolding@tamu.edu, morel@tamu.edu

INTRODUCTION

Accurate solution to the thermal radiative transfer (TRT) equations is important in the high-energy, high-density physics regime, e.g., for inertial confinement fusion and astrophysics simulations. Moment-based hybrid Monte Carlo (MC) methods have demonstrated great potential for accelerated solutions to TRT problems. Such methods iterate between a high-order (HO) transport equation and a low-order (LO) system formulated with angular moments and a fixed spatial mesh. Physics operators that are too expensive for the HO solver to resolve directly, e.g., photon absorption and emission, are moved to the LO system. The lower-rank LO equations can be solved with Newton methods to allow for non-linearities in the LO equations to be efficiently resolved. The high-order (HO) problem is defined by the transport equation that models the photon radiation with sources defined by the previous LO solution. Solution to the HO problem is used to construct consistency terms that require the next LO solution to be consistent with the HO solution. These consistency terms preserve the accuracy of the MC solution method in the LO equations, upon nonlinear convergence of the outer iterations.

Previously, residual Monte Carlo (RMC) methods have been used to provide efficient solution to the HO transport problem [1, **?**]; high-fidelity solutions, with minimal statistical noise, have been achieved for problems with optically-thick, diffusive regions that lead to slowly varying solutions. However, the results in these works used a backward Euler (BE) discretization for the time variable, which can inaccurately disperse radiation wavefronts in optically thin problems. We have extended the work in [**?**] to include higher-accuracy treatment of the time variable for the radiation unknowns. The exponentially-convergent Monte Carlo (ECMC) algorithm [**?**] was modified to include integration of the time variable; this includes the introduction of a step, doubly-discontinuous (SDD) trial space representation in time. A new parametric closure of the LO equations, introducing additional time-closure consistency terms, was derived to capture the time accuracy of the HO ECMC simulations. The LO equations can preserve the accuracy of MC radiation transport treatment in time, with the same numerical expense as Backward Euler (BE) time discretized S_2 equations. We have derived the LO equations directly from the transport equation, such that, neglecting spatial discretization differences, the HO and LO solutions are consistent upon convergence. Herein we briefly describe the HO and LO solvers, and we preset results for one-dimensional (1D), grey test problems. We compare our method to the implicit MC (IMC) method [2], the standard MC solution method for TRT problems.

METHODOLOGY

The 1D, grey TRT equations consist of the radiation and material energy balance equations, i.e.,

$$\frac{1}{c}\frac{\partial I(x,\mu,t)}{\partial t} + \mu\frac{\partial I(x,\mu,t)}{\partial x} + \sigma_a I(x,\mu,t) = \frac{1}{2}\sigma_a acT^4(x,t) \tag{1}$$

$$\rho c_v \frac{\partial T(x,t)}{\partial t} = \sigma_a \phi(x,t) - \sigma_a acT^4(x,t), \tag{2}$$

where physical scattering could optionally be included in Eq. (1), and appropriate initial and boundary conditions are specified. In the above equations x is the position, t is the time, μ is the x-direction cosine of the angular intensity $I(x,\mu,t)$, σ_a is the macroscopic absorption cross section (cm^{-1}), and a, c, ρ, and c_v are the radiation constant, speed of light, mass density, and specific heat, respectively. The desired transient unknowns are the material temperature $T(x,t)$ and the mean radiation intensity $\phi(x,t) = \int_{-1}^{1} I(x,\mu,t)d\mu$. The mean intensity is related to the radiation energy density E_r by the relation $E_r = \phi/c$. The equations can be strongly coupled through the gray Planckian emission source $\sigma_a acT^4$, which is a nonlinear function of temperature, and the absorption term $\sigma_a\phi$. In general, the material properties are a function of T.

In the HOLO context, the LO solver models the physical scattering and resolves the material temperature spatial distribution $T(x)$ over each time step. The HO solver computes angular and temporal relations for I. The fully-discrete LO equations are based on algebraic manipulations of exact moment equations, formed over a spatial finite-element (FE) mesh. The BE time discretization is applied to emission source throughout, but the radiation variables are left in terms of time-averaged and end-of-time-step unknowns. This is analogous to the time-integration in IMC [2]. Angularly, the LO radiation equations are similar to S_2 equations, with element-averaged consistency parameters that are weighted averages of μ. Additional consistency parameters are introduced in a parametric closure that eliminates the auxillary time-unknowns for radiation quantities. If the angular and time consistency parameters were estimated exactly, then the LO equations are exact moment equations, neglecting spatial discretization error. The consistency parameters are lagged in each LO solve, estimated from the previous HO solution for $I(x,\mu,t)$, as explained below. For the initial LO solve, within a time step, the angular parameters are calculated based on the $I(x,\mu)$ from the previous time step and the LO equations use a standard time discretization. The LO equations always conserve energy, independent of the accuracy of the consistency terms.

The solution to the LO system is used to construct a spatially linear-discontinuous (LD) FE representation of the emission source on the right hand side of Eq. (1). This defines

a fixed-source, pure absorber transport problem for the HO operator. This HO transport problem represents a characteristic method that uses MC to invert the continuous streaming plus removal operator with an LD representation of sources. We will solve this transport problem using the ECMC algorithm. The ECMC algorithm is an iterative residual MC (RMC) method, which uses batches of MC histories to estimate the error in the current trial-space representation of the $I(x, \mu, t)$. It is noted that because we are not using mesh adaptation in this work, exponential convergence in iterations cannot be maintained, but reduced variance from the RMC formulation can still be achieved. The output from ECMC is a projection $\tilde{I}(x, \mu, t)$ of the intensity onto the chosen trial space. This projection will accurately resolve the end-of-time step intensity. Once computed, $\tilde{I}(x, \mu)$ is used to directly evaluate the necessary LO angular consistency parameters and the time closure. The HO solution is not used to directly estimate a new temperature at the end of the time step; it is only used to estimate the parameters that go into the LO equations, which eliminates typical operator splitting stability issues that require linearization of the emission source.

The process of performing subsequential HO and LO solves occurs within a single time step, can be repeated to obtain an increasingly accurate solution for $\phi^{n+1}(x)$ and $T^{n+1}(x)$. However, for the problems tested here, only a single HO solve is performed during each time step. Thus, the HOLO algorithm, for the n-th time step, is

1. Perform a LO solve to produce an initial guess for $T_{LO}^{n+1}(x)$ and $\phi_{LO}^{n+1}(x)$, based on consistency terms estimated with $\tilde{I}^n(x, \mu)$ and a BE time discretization.

2. Solve the HO system for $\tilde{I}_{HO}(x, \mu, t)$ using ECMC, based on the current LO estimate of the emission and scattering sources.

3. Compute LO consistency parameters with $\tilde{I}_{HO}^{n+1}$.

4. Solve the LO system using HO consistency parameters to produce a new estimate of ϕ_{LO}^{n+1} and T_{LO}^{n+1}.

5. Store $\tilde{I}^n \leftarrow \tilde{I}^{n+1}$, and move to the next time step.

The LO System

To derive the LO equations, we reduce the dimensionality of Eq. (1) and Eq. (2) by taking spatial, angular, and temporal integrals. The spatial moments are taken over each spatial cell i: $x \in [x_{i-1/2}, x_{i+1/2}]$, weighted with the standard linear Lagrange interpolatory FE basis functions. For example, the left moment operator is defined by

$$\langle \cdot \rangle_{L,i} = \frac{2}{h_i} \int_{x_{i-1/2}}^{x_{i+1/2}} b_{L,i}(x)(\cdot)\mathrm{d}x, \qquad (3)$$

where $h_i = x_{i+1/2} - x_{i-1/2}$ is the width of the spatial element and $b_{L,i}(x) = (x_{i+1/2} - x)/h_i$ is the basis function corresponding to position $x_{i-1/2}$. Angularly, the equations are integrated over the positive and negative half ranges. The angular integrals of the intensity are defined as $\phi^{\pm}(x) = \pm 2\pi \int_0^{\pm 1} \psi(x, \mu)\mathrm{d}\mu$. Finally,

the equations are integrated over the n'th time step defined for $t \in [t^n, t^{n+1}]$ with width $\Delta t = t^{n+1} - t^n$.

The positive half-range integral, $\langle \cdot \rangle_{L,i}$ moment, and integration over a time step of Eq. (1) yields

$$\frac{\langle \phi \rangle_{L,i}^{+,n+1} - \langle \phi \rangle_{L,i}^{+,n}}{c\Delta t} - 2\overline{\mu}_{i-1/2}^{+}\overline{\phi}_{i-1/2}^{+} + \overline{\{\mu\}}_{L,i}^{+}\langle \overline{\phi} \rangle_{L,i}^{+} + \overline{\{\mu\}}_{R,i}^{+}\langle \overline{\phi} \rangle_{R,i}^{+}$$
$$+ \sigma_{a,i}^{n+1} h_i \langle \overline{\phi} \rangle_{L,i}^{n+1,+} = \frac{h_i}{2}\langle \sigma_a^{n+1} acT^{n+1,4} \rangle_{L,i}, \quad (4)$$

where overlined quantities denote time averaging. The time-averaged angular consistency terms are approximated with the previous HO solution, e.g.,

$$\overline{\{\mu\}}_{L,i}^{+} = \frac{\frac{2}{h_i} \int_0^1 \int_{x_{i-1/2}}^{x_{i+1/2}} \mu \, b_{L,i}(x)\overline{I}(x, \mu)\mathrm{d}x\mathrm{d}\mu}{\frac{2}{h_i} \int_0^1 \int_{x_{i-1/2}}^{x_{i+1/2}} b_{L,i}(x)\overline{I}(x, \mu)\mathrm{d}x\mathrm{d}\mu}. \qquad (5)$$

where $\overline{I}(x, \mu)$ is a time-averaged LDFE projection in x and μ, as explained in the next section. For simplicity, the face terms are eliminated from the system using a LDFE spatial approximation, with upwinding. There is some inconsistency introduced in this approximation, but it has proven stable for problems tested and demonstrates preservation of the equilibrium diffusion limit [3].

The LO equations must now be closed in time consistently with the HO equations. Previous work has enforced consistency in time by adding a local artificial source to the time-discretized LO equations in each cell [4]. This source was approximated based on the difference between the exact HO integral of the time derivative and the approximate BE representation in LO equations. We will alternatively use a parametric closure for the radiation unknowns.

Quantities at t^n are known from the previous time step or an initial condition. So Eq. (4) can be written exclusively in terms of time-averaged radiation unknowns, if $\langle \phi \rangle_{L,i}^{n+1}$ is eliminated from the system. The simplest closure is a weighted average

$$\langle \phi \rangle_{L,i}^{+,n+1} \approx \gamma_{L,i,HO}^{+}\langle \phi \rangle_{L,i}^{+} \qquad (6)$$

where $\gamma_{L,i,HO}^{+}$ is a time-closure consistency parameter. The above equation can be solved for the consistency parameter using moments of $\overline{I}_{HO}(x, \mu)$ and $I_{HO}^{n+1}(x, \mu)$. For the first solve during a time step, all γ values are set to unity, producing a BE discretization. but other closures, such as a modified Crank-Nicolson have been explored. In optically thin problems, the problem is nearly linear, and the choice of this closure becomes relatively arbitrary since all other unknowns have been eliminated from the system. Once the time-averaged unknowns have been calculated, the local time closures can be used to convert the time-averaged unknowns to end-of-time-step values. There are four time-closure consistency parameters, for each LO element.

The other radiation and material energy equations can be derived analogously. More specifics on the angular and spatial manipulation of equations can be found in [?]. Summing the equations over all cells, a global, nonlinear LO system of

equations is formed for the moment unknowns. This system of equations is solved using an analytic Newtons method, as in previous work [?]. We have also investigated the use of source iteration with an approximate diffusion synthetic acceleration method [?] to invert the scattering operator within Newton iterations [?].

The Residual MC High Order Solver

The transport equation to be solved by ECMC is given by Eq. (??), but with a known LDFE Planckian emission source:

$$\mathbf{L}I(x,\mu,t) = q_{LO}(x) \tag{7}$$

where q_{LO} denotes the latest estimate of the isotropic emission source, using $T_{LO}^{n+1}(x)$. The *continuous* linear operator $\mathbf{L}$ includes the streaming, removal, and time derivative on the left-hand side of Eq. (??).

To apply the residual MC algorithm, it is necessary to have a trial space representation of the solution for all phase space variables. The intensity is represented in x and μ with a LDFE projection [?]. This projection preserves the zeroth, and first moment in x and μ, over each space-angle cell. A step, doubly-discontinuous (SDD) trial space is used to represent the intensity as a function of t. The trial space representation for $I(x,\mu,t)$ is then

$$\tilde{I}(x,\mu,t) = \begin{cases} \tilde{I}^n(x,\mu) & t = t^n \\ \bar{I}(x,\mu) & t^n < t < t^{n+1} \\ \tilde{I}^{n+1}(x,\mu) & t = t^{n+1} \end{cases} \tag{8}$$

where we have used $\bar{I}$ to denote the time-averaged LDFE *projection* in x and μ of the intensity over the interior of the time step; the LDFE projections at t^n and t^{n+1} are denoted $\tilde{I}^n$ and $\tilde{I}^{n+1}$, respectively. The SDD trial space provides a projection for all the desired unknowns that result from time-integration of the transport equation to produce a balance equation, i.e., the time-averaged, end of time step, and previous time step intensities. Another benefit of this trial space is it allows for infrastructure for sampling from residual from the time-discrete formulation to be used directly. A drawback of the RMC approach is that a truncation error occurs by keeping only the LDFE projection of the intensity between time steps. Adaptive mesh refinement is likely necessary to capture highly-peaked solutions, but this could be included in the iterative ECMC algorithm.

To define the ECMC algorithm, we note that q_{LO} remains constant over the entire HO solve. The m-th approximate solution to Eq. (7) is $\tilde{I}^{(m)}$, where m identifies the MC batch. The m-th residual is $r^{(m)} = q - \mathbf{L}\tilde{I}^{(m)}$, which with manipulation gives the error equation

$$\mathbf{L}(I - \tilde{I}^{(m)}) = \mathbf{L}\epsilon^{(m)} = r^{(m)} \tag{9}$$

where I is the exact solution (for the problem which includes projection error of the previous time step) and $\tilde{\epsilon}^{(m)}$ is finite element representation, in space and angle, of the error in $\tilde{\psi}^{(m)}$. The above equation represents an auxiliary, fixed-source, pure absorber transport equation. The operator $\mathbf{L}$ is inverted without discretization via MC simulation to produce an estimate

of the error in $\tilde{\psi}^{(m)}$, i.e., $\tilde{\epsilon}^{(m)} = \mathbf{L}^{-1}r^{(m)}$. The MC simulation samples particles from the source $r^{(m)}$, which produces negative and positive weights. Histories are tracked in space, angle, and time, as for IMC [2]. The LDFE projection $\bar{\epsilon}$ is computed using generalized volumetric path-length estimators. A generalization of tallies used to estimate volume-averaged census energy from IMC [2] is used to capture the LDFE projection $\epsilon^{n+1}(x,\mu)$. The estimators are weighted by appropriate basis functions to tally the zeroth and first moments, in x and μ, of $I(x,\mu)$ over each space-angle cell.

Sampling from the residual is extended to the time variable from previous work. It is noted that the discontinuities in the trial space introduce δ-function sources because of $\frac{\partial \tilde{I}}{\partial t}$. However, the contribution from the discontinuity source at t^n can be analytically estimated such that it does not need to be sampled; the result is that $\tilde{I}^{n+1}$ is error particles that reach the time step and $\bar{I}^{(m)}(x,\mu)$.

The ECMC algorithm is

1. Solve Eq. (7) to compute the MC projection of the angular flux onto the LD $x - \mu$ trial space $\tilde{\psi}^{(0)}$.

2. Compute $r^{(m)}$.

3. Estimate $\tilde{\epsilon}^{(m)} = \mathbf{L}^{-1}r^{(m)}$ with N Monte Carlo histories.

4. Compute $\tilde{I}^{(m+1)} = \tilde{I}^{(m)} + \tilde{\epsilon}^{(m)}$

5. Optionally repeat 2 – 4 for desired number of batches.

RESULTS AND ANALYSIS

We have simulated two 1D, grey test problems to demonstrate the efficacy of our HOLO algorithm: an optically thin problem and a standard Marshak wave which provides a mix of thick and thin regions. Solutions are compared to results from a production IMC code [?]. We use a relative L_2 norm of the variance in spatially averaged radiation energy densities, E_r^{n+1}. The variance measure is The variance of a particular cell-averaged $\phi(x)$ is

$$S_i^2 = \frac{20}{20 - 1} \sum_{l=1}^{20} \left(\overline{\phi}_i - \phi_i^l\right)^2, \tag{10}$$

where ϕ_i^l is the cell-averaged scalar intensity for cell i from the l-th of 20 independent simulations and $\overline{\phi}_i$ is the corresponding sample mean from the 20 simulations. To provide a normalized, spatially-integrated result, we form a norm over cells as

$$\|s\| = \left(\frac{\sum\limits_{i=1}^{N_c} S_i^2}{\sum\limits_{i=1}^{N_c} \overline{\phi}_i^2} \right)^{1/2}, \tag{11}$$

where N_c is the number of spatial cells.

We will also form a figure of merit (FOM) to demonstrate how statistical accuracy scales with the number of histories performed. Our FOM is defined as

$$\text{FOM} = \frac{1}{N_{\text{tot}}\|s\|^2} \tag{12}$$

where N_{tot} is the total number of histories performed over the simulation. All FOM results are particular to a problem, and normalized to an IMC simulation.

Optically Thin Problem

For this problem, material properties are uniform throughout a 2.0 cm wide domain with $\rho c_v = 0.01374$ GJ cm^{-3} keV^{-1}, and $\sigma_a = 0.2$ cm^{-1}. The material and radiation are initially in equilibrium at an effective temperature of 0.01 keV. An isotropic incident intensity with $T_r = 0.150$ keV is applied at $x = 0$ for $t > 0$; the incident intensity on the right boundary is 0.01 keV. Solutions are depicted as an effective radiation temperature $T_r = (\phi/(ac))^{0.25}$; the values for T_r^{n+1} from the last time step are compared for IMC, the HOLO method with continuous time treatment (HOLO-TC), and the HOLO method with full BE time discretization (HOLO-BE) in Fig. 1. The HOLO-TC and HOLO-BE results were generated with 30 μ cells, and all spatial meshes used 200 cells. At smaller time step sizes, the effects of projecting the solution become apparent in the HOLO-TC results, leading to more dispersion near the wave-front. For $\Delta t = 0.005$ sh, there is good agreement between the HOLO-TC results and IMC. The HOLO-BE results do not accurately capture the wavefront location, as expected. IMC demonstrates noise in the equilibrium regions of the problem.
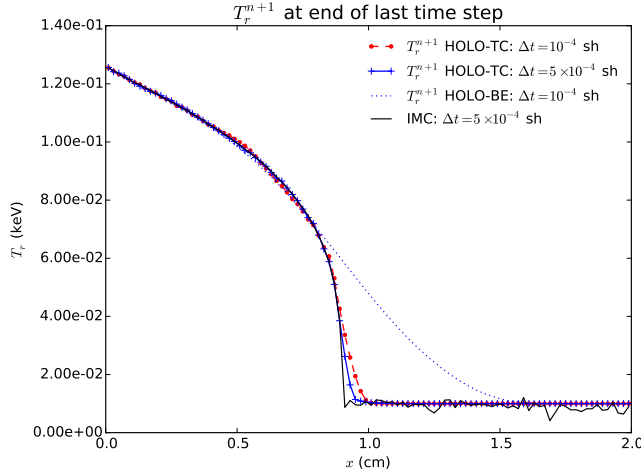

Fig. 1. Comparison of radiation temperatures for optically thin problem.

Table. **??** compares computed FOM values for the census radiation energy densities, for the case of $\Delta t = 0.0005$ sh. HOLO results were generated for the case of 1 and 2 batches, with the same total number of histories per time step. At low particle counts for the larger time step size, the HOLO-TC method demonstrates substantial noise. This is due to the trial space representation of the census particles at the end of the time step being poorly estimated. For the 2 batch case, the estimate from the first batch leads to less error in the census estimate as the ECMC solves are simply solving for the deviation from the time-averaged quantities of the first batch. The results for the case of 30,000 histories are plotted in Fig. **??** for the HO and LO solution. As demonstrated, there seems to have been some instabilities introduced into the LO equations through noise; sufficient sampling of the census must occur. At smaller time-steps there is an increase in statistical efficiency, however the accuracy is reduced due

to an increase in projection error. A finer mesh size is needed to produce higher accuracy.

TABLE I. Comparison of sample statistics for E_r^{n+1} from last time step for the optically thin problem. Simulation end time is $t = 0.003$ sh.

	FOM		
	$\Delta t = 5 \times 10^{-4}$ sh		
hists./step	IMC	HOLO-TC(1)	HOLO-TC(3)
30,000	1.00	0.03	0.31
300,000	0.93	1.38	1.65
1,000,000	1.10	3.42	2.0
	$\Delta t = 10^{-4}$ sh		
hists./step	IMC	HOLO-TC(1)	HOLO-TC(3)
30,000	1.00	29.81	5.51
300,000	0.98	71.82	9.88
1,000,000	1.11	71.02	9.71

Marshak Wave Problem

It is important to demonstrate that the time closures are stable in a mix of optically thick and optically thin regions, and that the ECMC method is still efficient in such problems. This problem has the same material properties as the previous, except the Marshak wave problem defined in Sec. **??**. The time step size is linearly increased from 0.001 sh to a maximum step of 0.01 sh over the first 10 time steps; the last time step is adjusted to reach the desired simulation end time. It was found for this problem that it was necessary to use more than one batch for the HOLO-TC algorithm to stably converge. This is because in the case of a single batch particles must reach census to accurately estimate the next time step value. These results were generated using the implicit-like time closure.
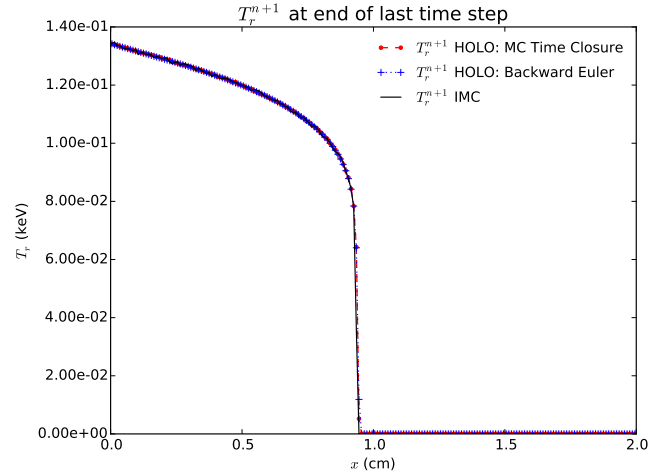

Fig. 2. Comparison of HOLO-TC, HOLO-BE, and IMC methods for the Marshak Wave problem, with 10^6 histories per time step.

Figure 2 compares the accuracy of IMC, HOLO-TC, and HOLO-BE. The solutions are plotted at $t = 3$ sh, with 10^6 histories per time step for all simulations. As demonstrated,

there is good agreement among the results. It is noted that this problem can be accurately modeled with the Backward Euler time discretization, but the MC time closure demonstrates stability in a mix of optically thick and thin regions. Table II compares sample statistics for IMC and the HOLO method with continuous time treatment and for a BE discretization. As demonstrated, at the lower history count (300,000), the HOLO-TC algorithm demostrates a much greater variance.

TABLE II. Comparison of sample statistics for the end of time step radiation energy densities, of the last time step, for the marshak wave problem and maximum time step of 0.01 sh. Simulation end time is $t = 3.0$ sh.

hists./step	$\|s\|$			FOM		
	IMC	HOLO-TC (2)	HOLO-BE (2)	IMC	HOLO-TC(2)	HOLO-BE (2)
300,000	2.25%	3.42%	0.30%	1.00	0.43	2050
1,000,000	1.27%	0.31%	0.17%	0.94	15.95	1806
Diamond Like Closure						
300,000	–	3.53%	–	–	0.41	–
1,000,000	–	0.37%	–	–	10.94	–

Later on, we can include a table, even one that spans two columns such as Table III.

CONCLUSIONS

Initial results demonstrate that residual MC methods can be extended to include the time variable. Our ECMC algorithm can be more statistically efficient than IMC, although a high mesh resolution is needed between time steps; adaptive mesh refinement would be highly beneficial for realistic applications. We have demonstrated a new approach to closing the LO equations that produces consistent solutions. Long-term, an alternative approach would be to operator split the census radiation.

At this point, we believe that the SDD trial space in time suffers from the fact that particles must reach the end-of-time step to contribute to the intensity, and ultimately the closure. Alternatively, the LDFE trial space could also include the time variable (i.e., it is linear in time). This has the added benefit that the slope can be estimated over the interior of the time-step, so all particle tracks contribute to the score. However, there is some additional truncation error as the end of time-step is an extrapolated quantity. We are investigating the use of the LD trial space, but it requires substantial modifications to the residual sampling algorithm because analytic L_1 integrals of the local residuals become untenable. An importance sampling methodology has been developed but remains to be implemented. Additionally, modifications to the sampling algorithm are necessary to extend to higher spatial dimensions or polynomial order, so determining if our approach is efficient will be of benefit to future work. We plan to include results for the LD representation in time for the full paper.

ACKNOWLEDGMENTS

REFERENCES

1. J. WILLERT and H. PARK, "Residual Monte Carlo High-order Solver for Moment-Based Accelerated Thermal Radiative Transfer Equations," *Journal of Computational Physics*, **276**, 405 – 421 (2014).
2. A. B. WOLLABER, "Four decades of implicit Monte Carlo," *Journal of Computational and Theoretical Transport*, **45**, *1-2*, 1–70 (2016).
3. J. MOREL, T. WAREING, and K. SMITH, "Linear-Discontinuous Spatial Differencing Scheme for S_n Radiative Transfer Calculations," *Journal of Computational Physics*, **128**, 445–462 (1996).
4. A. B. WOLLABER, H. PARK, R. LOWRIE, R. RAUEN-ZAHN, and M. CLEVELAND, "Radiation Hydrodynamics with a High-Order, Low-Order Method," in "ANS Topical Meeting, International Topical Meeting on Mathematics and Computation," Nashville Tennessee (2015).
5. E. WOLTERS, *Hybrid Monte Carlo - Deterministic Neutron Transport Methods Using Nonlinear Functionals*, Ph.D. thesis, Michigan (2011).

	$\phi_T(0)$	$\phi_T(10)$	$\phi_T(20)$	$\phi_D(0)$	$\phi_D(10)$	$\phi_D(20)$	ρ	ε	N_{it}
$c = 0.999$	0.9038	20.63	31.24	0.9087	20.63	31.23	0.2192	10^{-7}	15
$c = 0.990$	0.3675	13.04	24.7	0.3696	13.04	24.69	0.2184	10^{-7}	15
$c = 0.900$	0.009909	4.776	17.64	0.009984	4.786	17.63	0.2118	10^{-7}	14
$c = 0.500$	6.069×10^{-5}	2.212	15.53	6.213×10^{-5}	2.239	15.53	0.2068	10^{-7}	13

TABLE III. This is an example of a really wide table which might not normally fit in the document.